Proceedings of the ASME 2010 3rd Joint US-European Fluids Engineering Summer Meeting and 8th International Conference on Nanochannels, Microchannels, and Minichannels
FEDSM-ICNMM2010
August 1-5, 2010, Montreal, Canada

FEDSM-ICNMM2010-30764

EXPERIMENTAL INVESTIGATION OF TURBULENT BOUNDARY LAYERS UNDER FAVORABLE PRESSURE GRADIENT

Pranav Joshi
Johns Hopkins University
Baltimore, MD, USA

Joseph Katz
Johns Hopkins University
Baltimore, MD, USA

ABSTRACT

The goal of this research is to study the effect of favorable pressure gradient (FPG) on the near wall structures of a turbulent boundary layer on a smooth wall. 2D-PIV measurements have been performed in a sink flow, initially at a coarse resolution, to characterize the development of the mean flow and (under resolved) Reynolds stresses. Lack of self-similarity of mean velocity profiles shows that the boundary layer does not attain the sink flow equilibrium. In the initial phase of acceleration, the acceleration parameter, $K=\nu/U^2 dU/dx$, increases from zero to 0.575×10^{-6}, skin friction coefficient decreases and mean velocity profiles show a log region, but lack universality. Further downstream, K remains constant, skin friction coefficient increases and the mean velocity profiles show a second log region away from the wall. In the initial part of the FPG region, all the Reynolds stress components decrease over the entire boundary layer. In the latter phase, they continue to decrease in the middle of the boundary layer, and increase significantly close to the wall (below $y\sim0.15\delta$), where they collapse when normalized with the local freestream velocity. Turbulence production and wall-normal transport, scaled with outer units, show self-similar profiles close to the wall in the constant K region. Spanwise-streamwise plane data shows evidence of low speed streaks in the log layer, with widths scaling with the boundary layer thickness.

NOMENCLATURE

H	= boundary layer shape factor
h	= half channel height
K	= acceleration parameter
K_p	= pressure gradient parameter
L	= $[-\langle u'v'\rangle]^{1/2}/(\partial U/\partial y)$, mixing length
l	= length of the FPG region
P	= mean pressure
Re_θ	= $U_0(x)\theta(x)/\nu$, local momentum thickness Reynolds number
U	= mean streamwise velocity
U_0	= local freestream velocity
$U_{0,1}$	= freestream velocity at reference location x/l=-0.04
u',v',w'	= velocity fluctuations in the streamwise, wall-normal and spanwise directions respectively
u_τ	= local friction velocity
V	= mean wall-normal velocity
W	= mean spanwise velocity
x,y,z	= coordinates in streamwise, wall-normal and spanwise directions respectively
δ	= boundary layer thickness
δ^*	= $\int_0^\delta (1-U/U_0)dy$, displacement thickness
θ	= $\int_0^\delta U/U_0\,(1-U/U_0)dy$, momentum thickness
κ	= Karman constant in the universal log law for the mean velocity profile
ν	= kinematic viscosity
ρ	= fluid density

INTRODUCTION

Turbulent boundary layers under favorable pressure gradients are encountered in numerous configurations such as flow over airfoils, through turbine blade passages and nozzles. The strength of imposed acceleration on the flow and turbulence within a forward pressure gradient boundary layer can be defined by non-dimensional parameters, such as the acceleration parameter, K, or the pressure gradient parameter, K_p, defined as

$$K = \frac{\nu}{U^2}\frac{dU}{dx}, \quad K_p = \frac{\nu}{\rho u_\tau^3}\frac{dP}{dx} \qquad (1)$$

Under strong FPG, a turbulent boundary layer may relaminarize, as first reported by Sternberg in 1954 for a supersonic flow (Badri Narayanan and Ramjee, [1]). Thereafter, numerous studies of relaminarizing incompressible boundary layers have been performed, for e.g., Patel and Head, Blackwelder and Kovasznay, Escudier *et al*., Ichimiya *et al*., Talamelli *et al*., and Piomelli *et al*. [2-7]. In a comprehensive review, Sreenivasan [8] describes the various regimes a turbulent boundary layer goes through as it relaminarizes under a favorable pressure gradient. Under very mild pressure gradients, the boundary layer properties are almost the same as those of a zero pressure gradient, ZPG, boundary layer. As K increases, but not to the level of relaminarization, there is an intermediate stage, the so-called 'laminarescent' state, for which the boundary layer is still fully turbulent, but the turbulence structure is very different from that of a ZPG case (Spalart [9], Fernholz and Warnack [10]). A laminarescent boundary layer can still be in equilibrium, in the sense that the mean velocity and Reynolds stress profiles are self-similar when appropriately non-dimensionalized (Townsend [11]), if K does not vary rapidly in the streamwise direction. When K changes rapidly in comparison to local flow time scales, no equilibrium is possible. Relaminarization occurs when $K>\sim 3\times10^{-6}$ is maintained for a sufficient time or streamwise length (Spalart [9]).

An accelerated turbulent boundary layer typically features an increase in the coefficient of friction, a decrease in the shape factor, H, as the mean velocity profile becomes fuller (Sreenivasan [8]), and deviation of the mean velocity profile starts from the universal log law (Spalart [9], Jones and Launder [12]). Under equilibrium conditions (constant K), the profile is still logarithmic, but with constants that increasingly differ from those of the universal log law as K increases (Dixit and Ramesh [13]). Sreenivasan [8] also suggests the existence of a ½ power law in the mean velocity profile if the changes in the acceleration parameter are small, i.e. the boundary layer is in a "moving equilibrium". As the boundary layer starts relaminarizing, the turbulence level needs not be greatly diminished, but it is effectively overwhelmed by acceleration of the mean flow to affect the mean flow dynamics.

Trends of Reynolds stresses in different regions of a laminarescent boundary layer vary considerably in the literature, as discussed later in this paper. However, a consistently observed phenomenon is a significant rise in the turbulence levels very close to the wall. The causes for this 'normal' (Sreenivasan [8]) behavior are not yet understood. It is natural to expect that the changes in the turbulence structure close to the wall should be related to the dynamics of coherent structures there. It seems that important near-wall features of a turbulent boundary layer, which are generally agreed upon, include coherent quasi-streamwise vortical structures, including hairpin vortices, and the associated streamwise low speed streaks (Robinson [14], Panton [15], Adrian [16]). The dynamics of these turbulent structures strongly affect the production and dissipation of turbulence in the flow. Limited evidence has shown that during relaminarization, the low speed streaks become longer and have fewer undulations (Piomelli [7]). The bursting frequency also decreases (Ichimiya *et al*. [5], Kline *et al*. [17]). Talamelli *et al*. [6] observed an increase in the normalized (by wall units) spanwise spacing of the streaks, while Kline *et al*. [17] did not find any variations in spacing with pressure gradient. In case of equilibrium laminarescent boundary layers, Spalart [9], using DNS, observed at $K=2.5\times10^{-6}$ patches of quiescent fluid in the buffer layer ($y^+\sim11$) with lower wall stress, lower vorticity over the entire thickness of the boundary layer and a "smoother state of the flow in general" (Spalart [9]). The absolute streak spacing in these patches increased with decreasing wall shear stress. These patches were convected at 0.75 times the freestream velocity, with little change in their structure. These patches were not observed for a weaker $K=1.5\times10^{-6}$. Considering that the above references summarize the present state of knowledge, it is evident that we are still missing the fundamental knowledge needed for understanding the underlying physics of turbulence in an FPG boundary layer. The results presented in this paper represent early steps in our attempt to address this problem.

To maintain a constant strength of acceleration, we have opted to study a "sink flow" configuration, i.e. a constant K flow. This paper summarizes the findings from relatively coarse 2D-PIV measurements that cover the entire boundary layer, and follow the streamwise developments of the mean flow and Reynolds stress statistics. Samples of higher resolution data that focuses on the low speed streaks are also provided.

EXPERIMENTAL SETUP

Experiments were performed in a closed loop channel flow facility whose relevant section is illustrated in Fig. 1. This channel is an extension to the JHU optically index-matched test facility (Wu *et al*. [18]). The rectangular test section is 0.203 m wide and 0.051 m high. The channel is made of transparent acrylic, and the liquid, a concentrated solution of NaI in water (62% by weight), has almost the same optical refractive index as that of the acrylic walls to facilitate optical measurements very close to the wall. This liquid has a specific gravity of 1.8, and kinematic viscosity of 1.1×10^{-6}. The settling chamber upstream of the test section contains flow-straighteners, consisting of a honeycomb and screens, followed by a two-dimensional 4:1contraction. A second honeycomb B is installed at the beginning of the channel to minimize the effect of secondary channel flows on the measurements. Furthermore, a 0.002 m thick mesh is attached to the lower wall immediately downstream of the second honeycomb to trip the flow and enhance mixing, both of which improve the spanwise uniformity of the flow. The upper wall of the channel has a

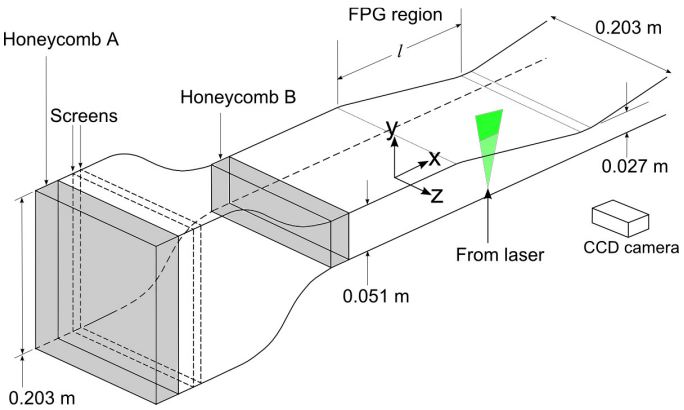

Figure 1. Schematic of the experimental facility

smooth transition to an inclined surface that generates a sink flow. Measurements are performed in the boundary layer on the lower wall. The height of the channel decreases from 0.051 m to 0.027 m over a streamwise length of l=0.313 m, henceforth called the FPG region. The X-axis is aligned in the streamwise direction and the Y-axis in the wall-normal direction. The streamwise distance is measured from the beginning of the FPG region.

Table 1. Different streamwise locations in the FPG region.

Location	x_1	x_2	x_3	x_4	x_5	x_6	x_7	x_8
x/l	-0.04	0.14	0.29	0.4	0.52	0.63	0.75	0.88
Resolution (μm)	383	383	344	344	300	300	249	249
Resolution (wall units)	--	53	48	40	44	54	50	60

For PIV measurements, the flow has been seeded with silver coated, 1-6 μm diameter, glass spheres that have a specific gravity of 2.6. The flow field is illuminated with an ~1mm thick laser sheet (Big Sky PIV120 laser, 120 mJ per pulse), and image pairs are recorded by a 4864 × 3248 pixels^2 Imperx IPX-16M3-L CCD camera (pixel pitch is 7.4 μm). The images are first enhanced using modified histogram equalization, and velocity is calculated using an in-house developed correlation based program (Roth *et al*. [19], Roth and Katz [20]). The interrogation window size is 32 × 32 pixels^2, with 50% overlap between windows. At least 5000 velocity distributions are used to obtain the flow statistics at each location. Images have been recorded at 8 different x-y planes along the streamwise direction. Data at one representative streamwise location for each plane is used in the following discussion. The field of view of the camera is adjusted to cover the entire boundary layer at any streamwise location. Consequently, four different magnifications are used, as summarized in Table 1, with the coarsest resolution in the first two locations, and the finest resolution near the exit from the accelerating region. The resolution at location x_1 is not provided in the table, as explained later. The locations of x_1-x_8 are sketched in Fig. 2. Higher resolution (198μm) data in the x-z planes, at the near-wall -<$u'v'$> peaks (shown later), has been obtained at selected streamwise locations of x/l=-0.04, 0.41 and 0.85. The interrogation window size for these cases is 48×48 pixels^2 with 50% overlap between the windows.

RESULTS AND DISCUSSION

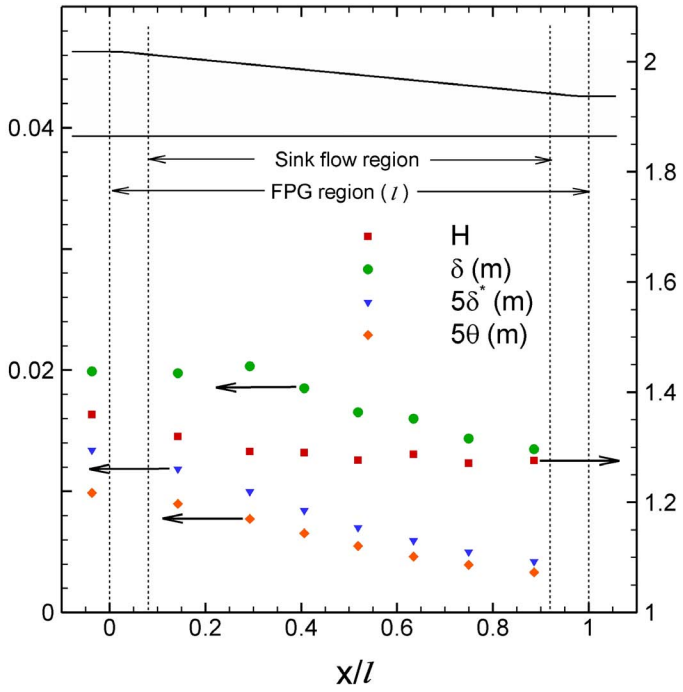

Figure 2. Variation of the boundary layer thicknesses and shape factor along the length of the FPG region.

Mean Flow

Figure 2 shows that δ^* and θ, which are defined in the nomenclature, decrease in the downstream direction, while δ shows a slight initial increase before dropping further downstream. In calculating the momentum and displacement thicknesses, the edge of the boundary layer (y=δ) is defined as the point where U/U_0=0.995. Because of the asymmetry in boundary conditions, $\partial U/\partial y$ outside of the boundary layer is very small (<0.3% of the maximum value) but non-zero. Consequently, $U_0(x)$ is based on values measured when $\partial U/\partial y$ decreases to a plateau of $0.025U_{0,1}/h$. The shape factor decreases slightly at the beginning of the contraction, as the mean velocity profiles become fuller in response to the imposed FPG, and then remains approximately constant. Its range of values, 1.36 - 1.27, is close to that observed in typical turbulent boundary layers (Pope [21], DeGraaff and Eaton [22]).

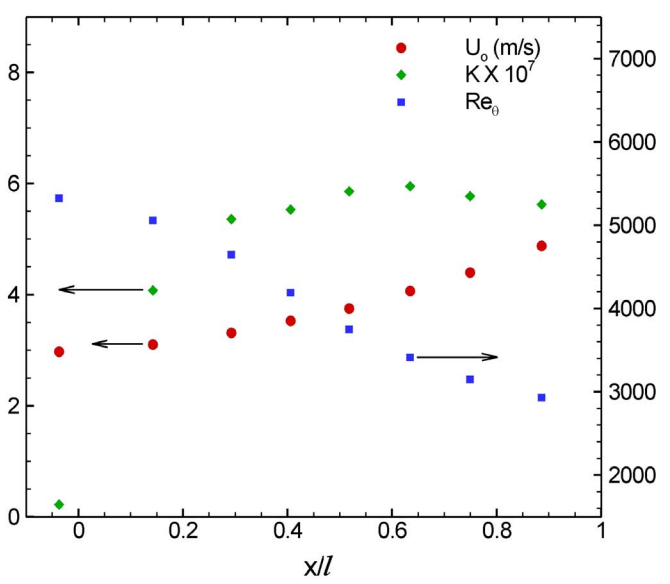

Figure 3. Variation of freestream velocity, acceleration parameter and local momentum thickness Reynolds number in the streamwise direction.

The developments of U_0, K, and Re_θ in the streamwise direction are shown in Fig. 3. The streamwise derivatives of U_0 and θ at each location are obtained by fitting a second order polynomial through that point and its two closest neighbors. As is evident from Fig. 3, K rises from nearly zero at x/l=-0.04, which is used as a reference for the flow before acceleration starts, to a plateau of ~ 0.575×10^{-6} at stations x/l=0.4-x/l=0.88. By construction, this value is well below the level required for flow relaminarization (Spalart [9]). Consequently, the boundary layer is expected to remain turbulent, yet it represents a significant departure from a ZPG turbulent boundary layer, as shown in the following discussion. The values of Re_θ, also shown in Fig. 3, decrease from 5325 at x/l=-0.04 to 2930 at x/l=0.88. Clearly, our sink flow region is not long enough for Re_θ to decrease to the equilibrium value of ~1700, as predicted for the present K by Jones *et al.* [23], based on the closure hypothesis of Perry *et al.* [24]. Mean non-dimensionalized velocity profiles at a few representative locations are shown in Fig. 4. All mean and turbulence profiles presented here have been obtained by averaging over 21 consecutive streamwise grid points (1.245-1.915 mm) centered at the particular x/l location. As expected, the mean velocity profiles become progressively fuller along the converging section, and do not collapse together, confirming that the boundary layer has not attained the sink flow equilibrium by the end of the FPG region.

To estimate the friction velocity, we use the boundary layer momentum integral equation,

$$\frac{u_\tau^2}{U_0^2} = \frac{d\theta}{dx} + (2\theta + \delta^*)\frac{1}{U_0}\frac{dU_0}{dx} \qquad (2)$$

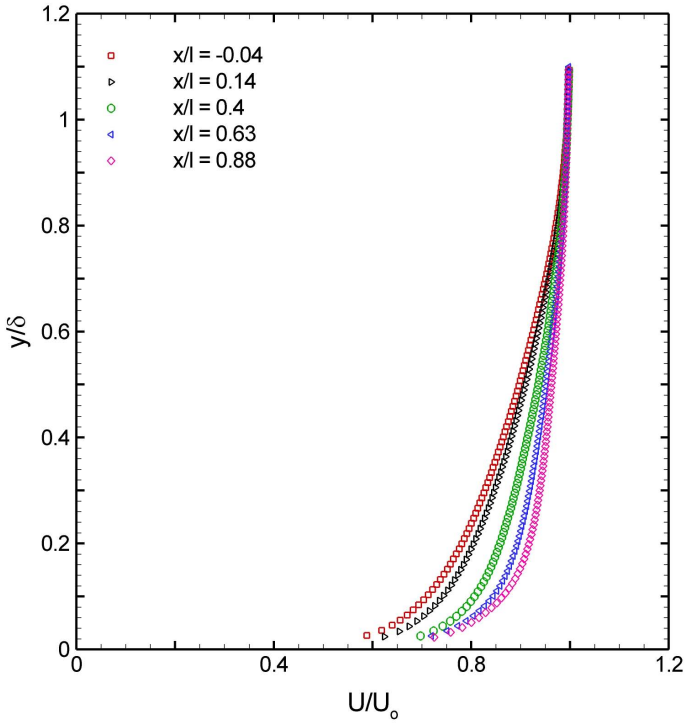

Figure 4. Mean velocity profiles at different streamwise locations.

We do not use the Clauser Chart method for calculating u_τ/U_0 since it assumes that the universal log law is valid. As discussed in Dixit and Ramesh [13], under equilibrium conditions, the Karman constant, κ, increases with K. Bourassa and Thomas [25] report that κ is very sensitive to dU_0/dx, especially at very low values, showing that κ can be as high as 0.58 for a modest K~0.6×10^{-6}. The accuracy of estimating u_τ/U_0 based on the use of Eq. 2 is affected by axial differentiation errors of U_0 and θ and the assumption that the flow is two-dimensional. The results for u_τ/U_0 presented in Fig. 5, and the PIV resolution in terms of wall units presented in Table 1 do not include the value at x/l=-0.04 since the streamwise derivative of θ there is very small and subject to high uncertainty. Within the sink flow, u_τ/U_0 initially decreases in the region where K increases rapidly, and subsequently increases again in the region of constant K. The initial decrease in u_τ/U_0 does not agree with trends reported in several studies describing the so-called "normal" response of a turbulent boundary layer to FPG (e.g., Badri Narayanan and Ramjee [1], Blackwelder and Kovasznay [3], Escudier *et al.* [4], Fernholz and Warnack [10]), but has been seen before during transitions to equilibrium conditions by, e.g. Jones et al. [23]. The reason for the initial decrease, which, as will be shown later, is consistent with trends of the Reynolds shear stress, is not clear to us. It is caused by the initial rapid decrease in momentum thickness. Effects of streamline curvature on the wall-normal pressure gradients, which are introduced by Sreenivasan [8] as a possible reason for secondary flows, are an order of magnitude smaller than

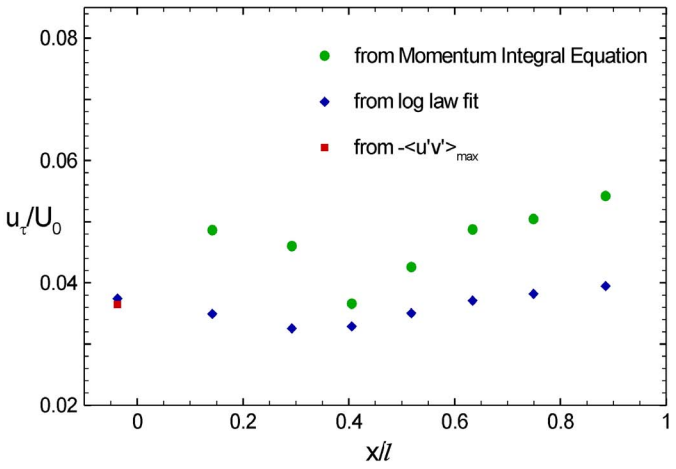

Figure 5. Variation of u_τ/U_0 along the length of the FPG region.

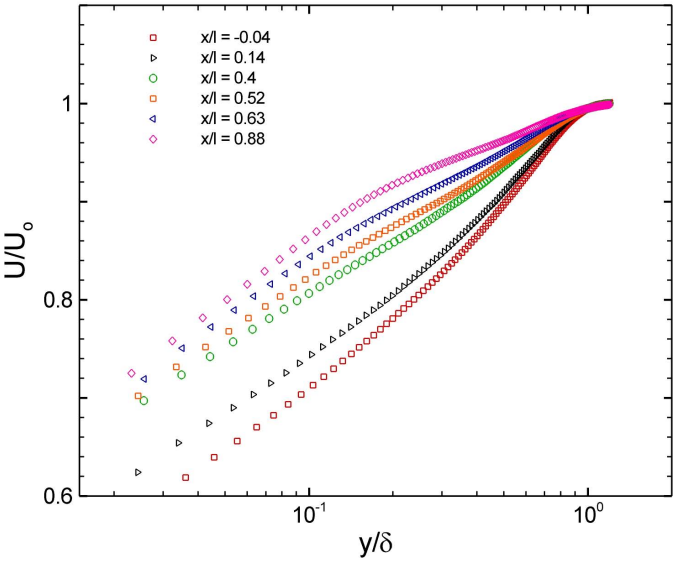

Figure 6. Mean velocity profiles showing logarithmic regions.

horizontal gradients near the lower wall of the present setup. For example, outside of the boundary layer, $\partial P/\partial y$ is about 20% of $\partial P/\partial x$ at x/l=0.14, but decreases to less than 5% at $x/l \geq 0.3$. Values of $V\partial U/\partial y$ are about 12% of $U\partial U/\partial x$ at the entrance to the converging section, but decrease to less than 5% at $x/l \geq 0.4$. Thus, effect of curvature cannot be ruled out at the entrance to the FPG region, but becomes quite small further inside. Furthermore, the x-z plane data does not show any significant spanwise flows, giving $(|W|/U)_{max} \sim 1\%$ over the entire channel within and outside of the lower boundary layer.

Sample mean velocity profiles, all showing logarithmic regions with fairly parallel slopes, are presented in Fig. 6. These profiles do not collapse when normalized by u_τ, with the normalized profile at x/l=0.4 being located far above the others due to the very low value of u_τ/U_0 there. The slopes of these profiles are lower than that prescribed by the universal log law, in line with numerous previous studies (Spalart [9], Jones and

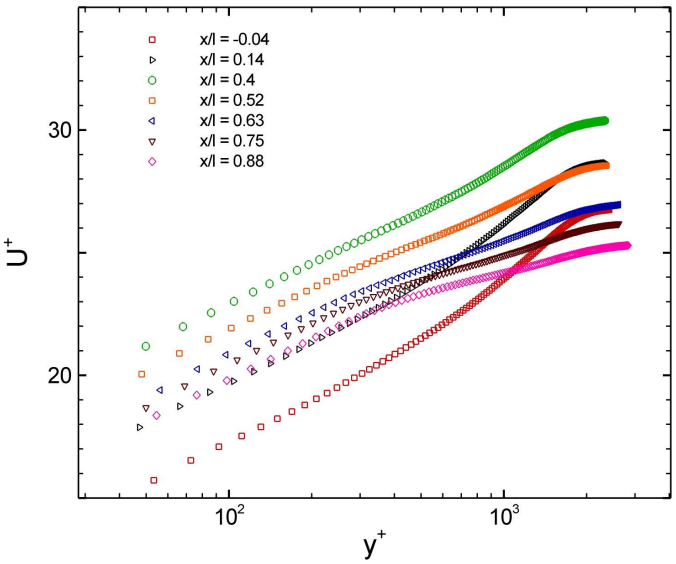

Figure 7. Mean velocity profiles normalized by wall units.

Launder [12], Dixit and Ramesh [13], Bourassa and Thomas [25]) showing that κ increases with increasing FPG. Using κ as a function of K, following Dixit and Ramesh [13], and fitting the data in the log region gives different estimates for u_τ/U_0, which are also presented in Fig. 5. As is evident, the two estimates for u_τ/U_0 differ by upto 40%, but the minimum near x/l=0.4 persists. An estimate for u_τ/U_0 at x/l=-0.04 from the peak value of $-\langle u'v' \rangle$ is also shown, and agrees well with the value obtained from the log law fit. As will be shown later, the minimum in u_τ/U_0 is located slightly upstream of a rapid increase in Reynolds shear stress very near the wall. Even with the lower values for u_τ/U_0 obtained from the log law fit, the non-dimensionalized profiles (Fig. 7) still do not collapse, especially in the region where K varies and curvature effects are not negligible, but show significantly better agreement at x/l>0.52, where K reaches a plateau. In the latter domain, the wake (outer) part of the mean velocity profile disappears, and is replaced with what appears to be a second logarithmic region with a lower slope. A dip of the mean velocity profile below the log law in non-equilibrium FPG boundary layers has been observed in several previous studies (e.g., Badri Narayanan and Ramjee [1], Patel and Head [2], Escudier *et al.* [4], Fernholz and Warnack [10]).

Turbulence Parameters and Structure

Reynolds stresses. Distributions of Reynolds stresses are shown in Fig. 8a-c, with the insets depicting a magnified view of the near-wall region. It is important to recall that these data are based on low resolution measurements of approximately 40-60 wall units. Consequently, the stresses are most likely underestimated, especially very close to the wall. Local freestream velocity is used for non-dimensionalization, in part since we are uncertain of the estimates for u_τ. All the profiles at

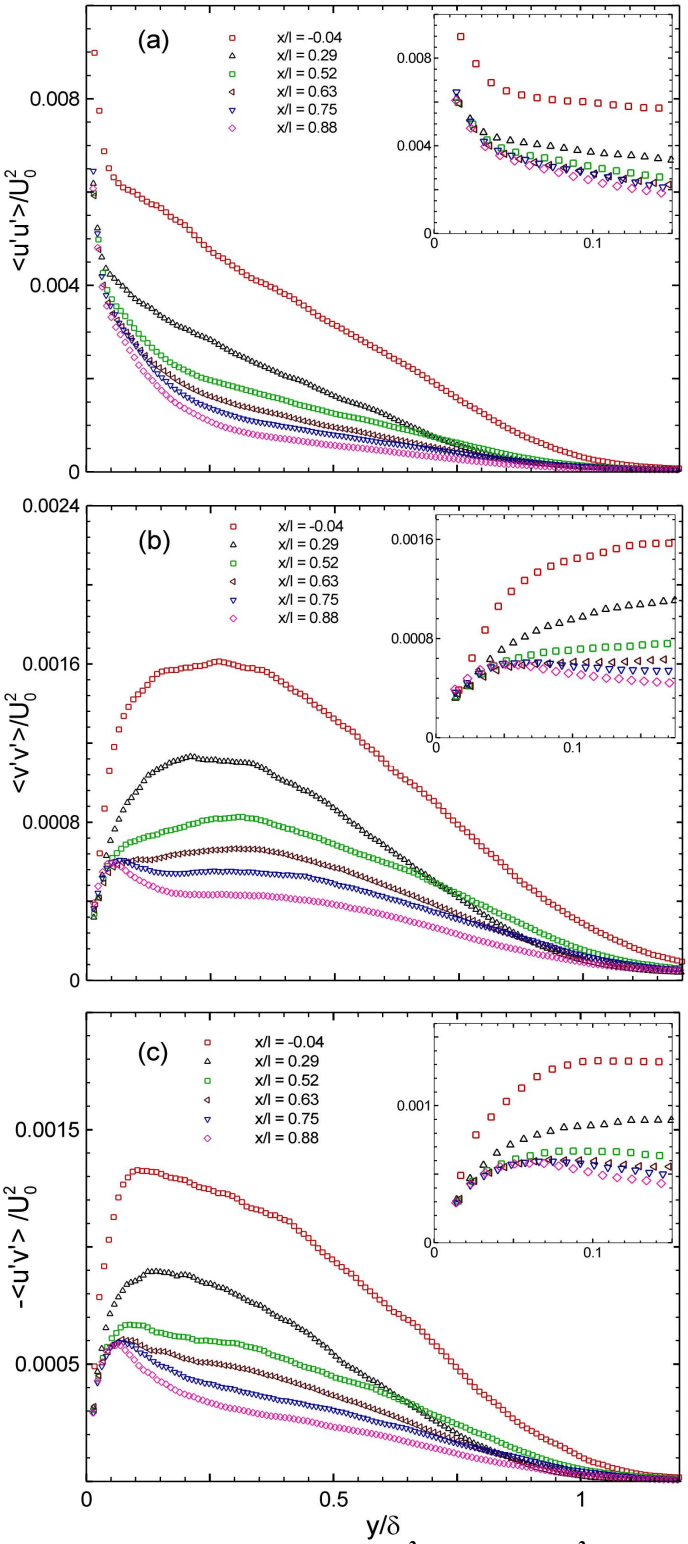

Figure 8. Profiles of (a) $\langle u'u' \rangle / U_o^2$, (b) $\langle v'v' \rangle / U_o^2$ and (c) $-\langle u'v' \rangle / U_o^2$. Insets show magnified views of the near-wall region.

x/l=-0.04 are similar to those observed in a typical ZPG turbulent boundary layer (DeGraaff and Eaton [22]).

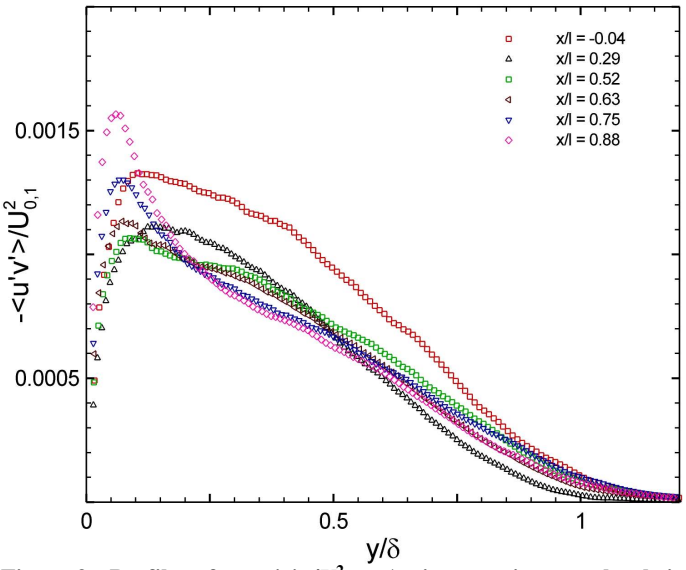

Figure 9. Profiles of $-\langle u'v' \rangle / U_{0,1}^2$. An increase in stress levels is seen in the near wall region at *x/l*=0.63-0.88.

All the stress components decrease over almost the entire boundary layer in the downstream direction, in agreement with trends reported previously in several studies (e.g., Jones and Launder [12], Ichimiya *et al.* [5]). This response of the stresses to FPG is opposite to that to a rough wall observed by Cal *et al.* [26]. Close to the wall (y/δ<0.15), the profiles collapse at the last few locations, i.e., in the region of constant *K*, indicating that stresses scaled with U_0^2 do not decrease near the wall. When $U_{0,1}$, the freestream velocity at station 1 (*x/l*=-0.04), is used as the constant velocity scale, Fig. 9 shows very different trends for the shear stress. Initially, in the *x/l*=-0.04 to 0.29 range, the magnitude of $-\langle u'v' \rangle$ decreases over the entire boundary layer. Further downstream, in the area where the skin friction starts increasing (*x/l*>0.4), the shear stress continues to drop in the middle of the boundary layer, but increases substantially close to the wall, with the peaks located within the logarithmic regions. The rapid increase near the wall is observed also for $\langle u'u' \rangle$ and $\langle v'v' \rangle$ (figures not shown), and as Fig. 8 shows, in all cases, the increase scales with the local freestream velocity (squared). Since $u_\tau(x)/U_0(x)$ increases with *x/l* (Fig. 5), the near wall stress profiles do not collapse when scaled with the friction velocity.

Most of the previous studies with constant *K* focus on the equilibrium state of the boundary layer. Among the studies reporting the evolution of stresses under a FPG with varying *K*, the trends of the magnitudes of Reynolds stresses in the outer region differ significantly, with some reporting an increase (e.g., Blackwelder and Kovasznay [3], De Prisco *et al.* [27]), while others reporting a decrease (e.g. Escudier *et al.* [4], Fernholz and Warnack [10]). However, most of these studies show an increase in the stress magnitudes very close to the wall (e.g., Blackwelder and Kovasznay [3], Escudier *et al.* [4], Piomelli *et al.* [7], Fernholz and Warnack [10], Bourassa and Thomas

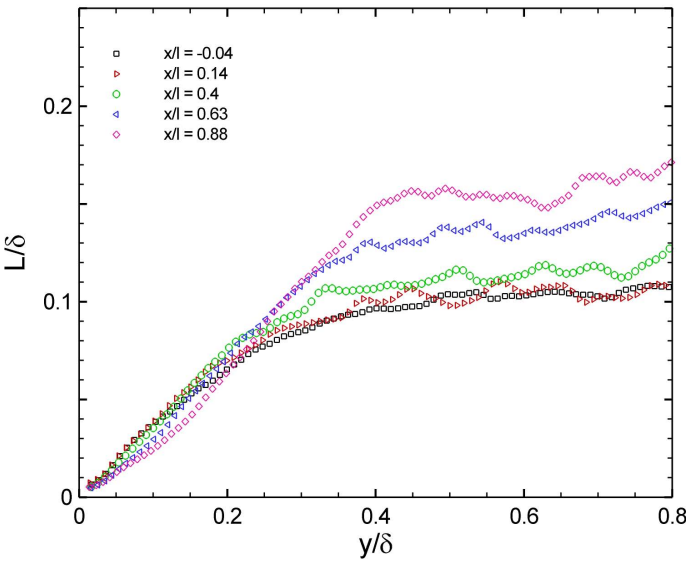

Figure 10. Mixing length at different streamwise locations.

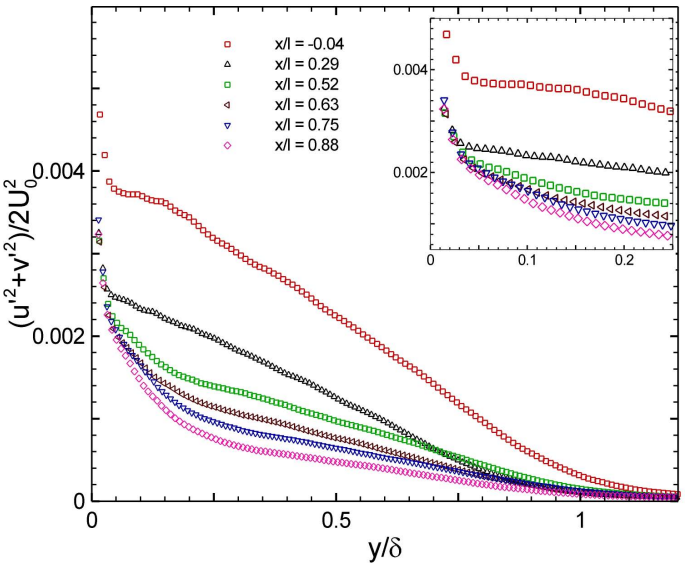

Figure 11. Profiles of turbulent kinetic energy.

[25]). Although commonly observed, this near-wall rise in the stresses is not understood.

When the shear stress profiles are compared to mean velocity gradients, e.g. by plotting the mixing length $L=[-<u'v'>]^{1/2}/(\partial U/\partial y)$ (Fig. 10), results show that the rapid increase in shear stress near the wall occurs coincidentally and is balanced by a rapid increase in mean velocity gradients. Values of L also increase with distance from the wall in the log layer, and plateau in the outer layer. In regions with a single log layer, the slope of L remains constant until the outer layer. Further downstream, when the outer layer disappears and is replaced by a second log layer (x/l=0.63-0.88, Fig. 6), the slopes of mixing length profiles shift to higher values in the second log layer. It should be noted that except for the increase in L with y, the present trends do not agree with results of DNS of an equilibrium sink flow reported by Spalart [9], for $K\sim1.5\times10^{-6}$.

Turbulent Kinetic Energy Budget. Profiles of turbulent kinetic energy (TKE) are presented in Fig. 11. Similar to the Reynolds stresses, $<u'^2+v'^2>/2U_0^2$ decreases over the entire boundary layer, except close to the wall, where the profiles collapse in the region of constant K. These trends of TKE agree with those of the dominant contributor to TKE production rate, namely $-<u'v'>\partial U/\partial y(\delta/U_0^3)$, which is shown in Fig. 12. The magnitude of the sum of the other production terms, also shown in Fig. 12, $-<u'u'>\partial U/\partial x$, $-<v'v'>\partial V/\partial y$, and $-<u'v'>\partial V/\partial x$, is small, but increases slightly near the wall due to acceleration. Its negative value indicates that it tends to transfer energy of turbulence back to the mean flow. However, the normalized $-<u'v'>\partial U/\partial y$ overwhelms all the other terms, giving a net production of TKE. Note that the non-normalized TKE and shear production close to the wall (not shown) decrease in the

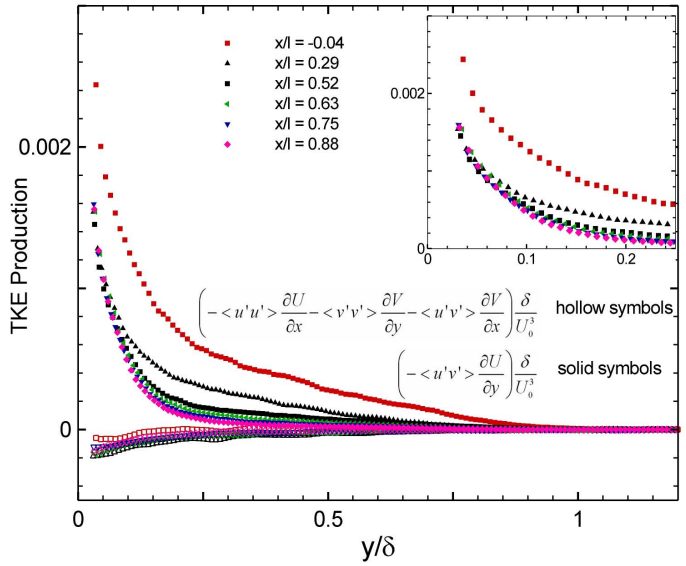

Figure 12. Profiles of TKE production rate. Close to the wall, TKE follows the trends in TKE production rate.

initial phase of the acceleration, and then increase further downstream, in the region of increasing skin friction (x/l>0.4), similar to the trends of Reynolds shear stress (Fig. 9). An increase in shear production close to the wall due to the imposed FPG is similar to data provided by Fernholz and Warnack [10], and Bourassa and Thomas [25].

The development of the wall-normal TKE transport, $-\partial<v'(u'^2+v'^2)/2>/\partial y(\delta/U_0^3)$, is shown in Fig. 13. Upstream of the FPG region (x/l=-0.04), scaled transport is positive in the outer parts, and negative in the inner parts, except below $y/\delta\sim0.06$, where our limited resolution prevents us from resolving the buffer layer. These trends are consistent with DNS data (Spalart [28]). Due to the FPG, transport becomes negative

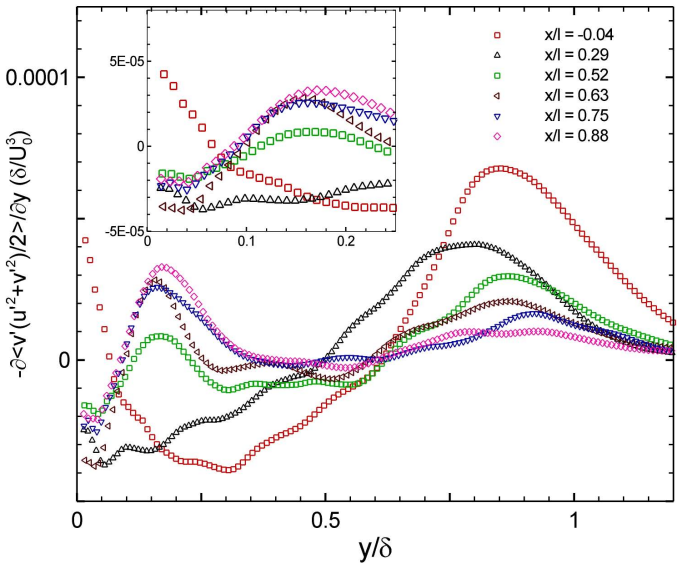

Figure 13. Profiles of the wall-normal turbulent transport.

very close to the wall, but the associated loss of TKE is much smaller than the production rate. Away from the wall (y/δ>0.1), there are two positive transport peaks. Similar to production rate, the normalized vertical transport profiles tend to collapse near the wall in the region of constant K. The streamwise transport of TKE increases due to the acceleration (figures not shown), but remains negligible compared to the wall-normal values.

Sample Data in the *x-z* Plane

Figures 14 a-b show samples of instantaneous u'/U fields in x-z planes located at x/l=-0.04 (y/δ=0.15) and x/l=0.85 (y/δ=0.07), respectively. These wall-normal locations are coincident with the peaks of the -<$u'v'$> profiles (Fig. 9). Streamwise and spanwise coordinates are provided both in actual dimensions as well as normalized by the corresponding boundary layer thicknesses. Existence of the so-called low speed streaks is clearly evident. As a qualitative assessment (analysis is still on-going), these elongated regions of negative and positive u' are present in a substantial fraction of the individual realizations. The magnitude of u'<0 peaks appear to be significantly stronger and their width narrower than those of the positive ones. As the two samples show, the low speed streaks are narrower at x/l=0.85 than those observed at x/l=-0.04. We are unable to determine the streamwise extent of these low speed regions, as most of these extend beyond the streamwise extent of the velocity field. Existence of low speed streaks and their role in turbulence dynamics in boundary layers has been discussed in numerous papers, e.g. Robinson [14], Panton [15], mostly for ZPG boundary layers, but also in FPG cases (e.g. Spalart [9], Piomelli *et al.* [7] and Talamelli *et al.* [6]). Hutchins and Marusic [29] recently observed that the

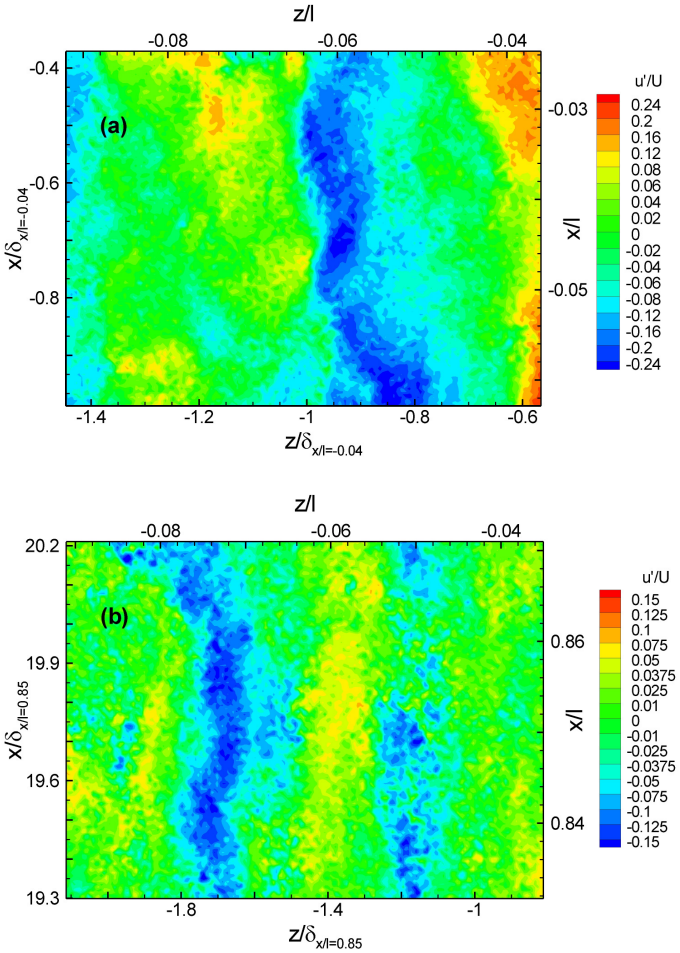

Figure 14. Instantaneous plots of u'/U fluctuations in the x-z plane at (a) x/l=-0.04, y/δ=0.15, and (b) x/l=0.85, y/δ=0.07.

"meandering" streaks in the log region of ZPG boundary layers have streamwise and spanwise scales of the order of 20δ and δ, respectively, the latter in agreement with both examples shown in Fig. 14. At least for the data that we have examined to-date, the width of streaks scales with the boundary layer thickness, even in accelerating flows.

CONCLUSIONS

This paper examines the effect of favorable pressure gradient on the mean flow and turbulence statistics of a turbulent boundary layer. Data are obtained by performing 2-D PIV measurements at a (relatively) coarse resolution. The boundary layer does not attain the sink flow equilibrium, which is evident from the lack of self-similarity of the mean velocity profiles. However, the latter part of the flow domain achieves a constant acceleration parameter, and indeed, variations in scaled mean velocity there are substantially smaller than those located upstream. There seem to be two different regimes over the length of the accelerating region. In the initial part, the

acceleration parameter rises, u_τ/U_0 decreases, and the mean velocity profiles have a logarithmic region, but with no universality. In the latter half, the acceleration parameter remains constant, u_τ/U_0 increases, the wake region in the outer parts of the boundary layer disappears, and seems to be replaced by a second log region. In the first part of the accelerating region, the magnitudes of all the measured Reynolds stresses decrease over the entire boundary layer. Conversely, in the second part, the Reynolds stresses still decrease in most of the outer layer, but near the wall, i.e. at y/δ<~0.15, all the stress components increase in the streamwise direction. When normalized with the local velocity outside of the boundary layer, the stresses decrease in outer parts of the boundary layer, but collapse onto the same profiles close to the wall. Furthermore, in this region, the TKE production rate and wall-normal transport near the wall also scale with U_0^3/δ. Since the estimated magnitudes of u_τ/U_0 in the constant K region increase in the axial direction, scaling of Reynolds stresses with the friction velocity does not provide collapsed results. Uncertainty in the method used to estimate the value of u_τ may also contribute to this discrepancy.

We are presently in the process of analyzing higher resolution data over the entire boundary layer that has been obtained in multiple directions. Consistent with scaling trends of Reynolds stresses, sample x-z plane data suggests that the widths of low speed streaks in the log layer scale with an outer layer parameter, namely the boundary layer thickness.

ACKNOWLEDGEMENT

The authors acknowledge the financial support from the National Science Foundation, initially under grant No. CTS 0625571, and continuing under grant No. CBET 0932941.

REFERENCES

[1] Badri Narayanan, M., A., and Ramjee, V., 1969, "On the Criteria for Reverse Transition in a Two-dimensional Boundary Layer Flow," J. Fluid Mech., **35**, part 2, pp. 225-241.

[2] Patel, V., C., and Head, M., R., 1968, "Reversion of Turbulent to Laminar Flow," J. Fluid Mech., **34**, part 2, pp.371-392.

[3] Blackwelder, R., F., and Kovasznay, L., S., G., 1972, "Large-Scale Motion of a Turbulent Boundary Layer during Relaminarization," J. Fluid Mech., **53**, pp. 61–83.

[4] Escudier, M. P., and Abdel-Hameed, A., Johnson, M. W., and Sutcliffe, C. J., 1998, "Laminarisation and Re-Transition of a Turbulent Boundary Layer Subjected to Favorable Pressure Gradient," Exp. Fluids, **25**, pp. 491–502.

[5] Ichimiya, M., Nakamura, I., and Yamashita, S., 1998, "Properties of a Relaminarizing Turbulent Boundary Layer Under a Favorable Pressure Gradient," Exp. Therm. Fluid Sci., **17**, pp. 37–48.

[6] Talamelli, A., Fornaciari, N., Johan, K., Westin, A., and Alfredsson, P., H., 2002, "Experimental Investigation of Streaky Structures in a Relaminarizing Boundary Layer," J. Turbulence, **3:1**, pp. 1-13.

[7] Piomelli, U., Balaras, E., and Pascarelli, A., 2000, "Turbulent Structures in Accelerating Boundary Layers," J. Turbulence, **1:1**, pp. 1-16.

[8] Sreenivasan, K., R., 1982, "Laminarescent, Relaminarizing and Retransitional Flows," Acta Mechanica, **44**, pp. 1-48.

[9] Spalart, P., R., 1986, "Numerical Study of Sink-flow Boundary Layers," J. Fluid Mech., **172**, pp. 307-328.

[10] Fernholz, H. H., and Warnack, D., 1998, "The Effects of a Favorable Pressure Gradient and of the Reynolds Number on an Incompressible Axisymmetric Turbulent Boundary Layer. Part 1. The Turbulent Boundary Layer," J. Fluid Mech., **359**, pp. 329–356.

[11] Townsend, A., A., 1956, "The Structure of Turbulent Shear Flow," Cambridge University Press, 1st Edition.

[12] Jones, W., P., and Launder, B., E., 1972 "Some Properties of Sink-flow Turbulent Boundary Layers," J. Fluid Mech., **56**, part 2, pp. 337-351.

[13] Dixit, S., A., and Ramesh, O., N., 2008, "Pressure-gradient-dependent Logarithmic Laws in Sink Flow Turbulent Boundary Layers," J. Fluid Mech., **615**, pp. 445-475.

[14] Robinson, S., K., 1991, "Coherent Motions in the Turbulent Boundary Layer," Annu. Rev. Fluid Mech., **23**, pp. 601-639.

[15] Panton, R., L., 2001, "Overview of the Self-sustaining Mechanisms of Wall Turbulence," Progress in Aerospace Sciences, 37, pp. 341-383.

[16] Adrian, R., J., 2007, "Hairpin Vortex Organization in Wall Turbulence," Phys. Fluids, 19, p. 041301.

[17] Kline, S., J., Reynolds, W., C., Schraub, F., A., Runstadler, P., W., 1967, "The Structure of Turbulent Boundary Layers," J. Fluid Mech., **30**, pp. 741-773.

[18] Wu, H., Miorini, R., L., Katz, J., 2010, "Measurements of the Tip Leakage Vortex Structures and Turbulence in the Meridional Plane of an Axial Water-Jet Pump," Expts. Fluids, submitted.

[19] Roth, G., I., Mascenik, D., T., Katz, J., 1999, "Measurements of the Flow Structure and Turbulence Within a Ship Bow Wave," Phys. Fluids, **11**, pp. 3512-3523.

[20] Roth, G., I., and Katz, J., 2001, "Five Techniques for Increasing the Speed and Accuracy of PIV Interrogation," Meas. Sci. & Tech., **12**, pp. 238-245.

[21] Pope, S., B., 2000, "Turbulent Flows," Cambridge University Press, 1st Edition.

[22] DeGraaff, D., B., and Eaton, J., K., 2000, "Reynolds-number Scaling of the Flat-plate Turbulent Boundary Layer," J. Fluid Mech., **422**, pp. 319-346.

[23] Jones, M., B., Marusic, I., and Perry, A., E., 2001 "Evolution and Structure of Sink-flow Turbulent Boundary Layers," J. Fluid Mech., **428**, pp. 1-27.

[24] Perry, A., E., Marusic, I., and Li, J., D., 1994, "Wall Turbulence Closure Based on Classical Similarity Laws and the Attached Eddy Hypothesis," Phys. Fluids, **6**, pp. 1024-1035.

[25] Bourassa, C., and Thomas, F., O., 2009, "An Experimental Investigation of a Highly Accelerated Turbulent Boundary Layer," J. Fluid Mech., **634**, pp. 359-404.

[26] Cal, R., B., Brzek, B., Johansson, T., G., and Castillo, L., 2009, "The Rough Favourable Pressure Gradient Turbulent Boundary Layer," J. Fluid Mech., **641**, pp. 129-155.

[27] De Prisco, G., Keating, A., Piomelli, U., Balaras, E., 2007, "Large-eddy Simulation of Accelerating Boundary Layers," Progress in Turbulence II, **Part IV**, Springer Berlin Heidelberg, pp. 137-143.

[28] Spalart, P., R., 1988, "Direct Simulation of a Turbulent Boundary Layer up to R_θ=1410," J. Fluid Mech., **187**, pp. 61-98.

[29] Hutchins, N., and Marusic, I., 2007, "Evidence of Very Long Meandering Features in the Logarithmic Region of Turbulent Boundary Layers," J. Fluid Mech., **579**, pp. 1-28.

